

POLITECNICO DI MILANO

POLO REGIONALE DI LECCO

MASTER OF SCIENCE IN MECHANICAL ENGINEERING



GEOMETRICAL OPTIMIZATION OF NOTCHES UNDER MULTI-AXIAL FATIGUE STRESSES

**SUPERVISOR: PROF. MARIO GUALIANO
CO-SUPERVISOR: INGEGNERE RAMIN GHELICHI**

MASTER THESIS SUBMITTED BY

RAHUL MAHADEV KUMBHAR [Matricola 749640]

ACADEMIC YEAR 2010/11

ABSTRACT

GEOMETRICAL OPTIMIZATION OF NOTCHES UNDER MULITI-AXIAL STRESSES

The objective of this study was to understanding the application of a geometrical optimization of notches under multi-axial fatigue stresses. There are ways to structural optimization criteria based on the Von-Mises equivalent stress are strictly applicable to static loading, and that their application to fatigue loading is questionable, particularly when the applied loads are out-of-phase, an approach based on Computer Aided Optimization proposed by Mattheck in the '90s of the last century is proposed. The original CAO method is modified by introducing the Liu-Zenner fatigue criterion. A numerical routine is developed that, by means of an interface to ABAQUS FE code, is able to lead to an optimized geometry of notched details under general multi-axial loading.

We applied this procedure on the automobile crankshaft to improve its fatigue life. This report presents the results of the same. It is found that this method is very useful and gives more accurate results than other available methods.

ACKNOWLEDGMENTS

I would like to thank Prof. Mario Guagliano to allow me to work on this innovative and interesting project. I am very thankful to engineer Ramin Ghelichi for his kind and informative guide and support. Both of them gave me a space to think individually and discuss frankly with them.

I would like to thank Erasmus Mundus-European Commission for granting me scholarship and assisting me financially. I also like to thank Politecnico di Milano for allowing me to study in the University.

Table of Contents

| | |
|--|----|
| Abstract..... | 1 |
| Acknowledgement..... | 2 |
| Table of contents..... | 3 |
| List of Tables..... | 4 |
| List of Figures | 5 |
| Nomenclature | 6 |
| 1. Introduction | 7 |
| 2. Optimization procedure | 10 |
| 2.1 Available methods | 11 |
| 2.2 Liu-Zenner Criterion..... | 15 |
| - Definition of shear stress amplitude and mean value..... | 17 |
| - The mean point method..... | 18 |
| 2.3 Optimization procedure..... | 20 |
| 3. Application | 23 |
| 3.1 Dynamic Load analysis..... | 23 |
| 3.2 Finite element modelling..... | 28 |
| 3.2.1 Geometry generation..... | 30 |
| 3.2.2 Mesh Generation..... | 34 |
| 3.2.3 Loading and Boundary conditions..... | 36 |
| 3.3 FEM Results..... | 38 |
| 3.4 Liu-Zenner equivalent stresses..... | 40 |
| 3.5 Virtual temperature distribution..... | 41 |
| 3.6 Applying nodal displacements..... | 43 |
| 3.7 Convergence..... | 43 |
| 4. Conclusion | 45 |
| References..... | 46 |

List of tables

Table 3.1 Details of slider crank mechanism used in ADAMS

Table 3.2 Configuration of Engine

Table 3.3 Material Properties of forged crankshaft

List of figures

Figure 2.1 Integration domain of the SIH and stress components in the intersection plane $\gamma\phi$.

Figure 2.2 Flowchart of the Modified CAO method.

Figure 3.1 Slider crank mechanism.

Figure 3.2 Slider crank mechanism used in ADAMS.

Figure 3.3 Pressure versus volume diagram.

Figure 3.4 Pressure versus crankshaft angle through one cycle.

Figure 3.5 Force versus crankshaft angle during 720 degrees for a engine having 3600 rpm.

Figure 3.6 Three different loadings on crankshaft bending (F_x), torsional (F_y), and longitudinal (F_z).

Figure 3.7 Solid model of Forged crankshaft generated in Catia-V5.

Figure 3.8 Actual picture of Forged steel Crankshaft.

Figure 3.9 Dimensional drawing of forged crankshaft.

Figure 3.10 Element sizes used at different locations for the forged steel crankshaft. (a) and (b) are front and back views respectively.

Figure 3.11 The meshed geometry of forged crankshaft.

Figure 3.12 The forged steel crankshaft in engine assembly taken from the engine manual of forged crankshaft.

Figure 3.13 Load and Boundary conditions at '0' degree.

Figure 3.14 Critical locations on the forged crankshaft

Figure 3.15 Maximum stress at the pin fillet and it is 118 MPa at the engine speed of 3500 rpm.

Figure 3.16 Critical fillet locations for shape modification

Figure 3.17 Shows the thermal distribution on nodes and change in shape. Original and deformed, both shapes are shown.

Figure 3.18 Shows both sets in un-deformed and deformed shapes.

Figure 3.19 Von-Mises stress convergence

Figure 3.20 Liu-Zenner stress convergence

Nomenclature

| Parameters | Description |
|--|---|
| N | Normal vector of material planes |
| ϕ, γ | Angles of normal vector in spherical coordinates |
| $\sigma_{va,\tau}, \sigma_{va,\sigma}$ | Equivalent shear and normal stress amplitude |
| $\sigma_{vm,\tau}, \sigma_{vm,\sigma}$ | Equivalent shear and normal mean stress |
| $\sigma_{va,\sigma}, \sigma_{vm,\sigma}$ | Shear stress amplitude and mean shear stress on each material plane |
| $\tau_{\gamma\phi a}, \tau_{\gamma\phi m}$ | Normal stress amplitude and mean stress on each material plane |
| $\sigma_{\gamma\phi a}, \sigma_{\gamma\phi m}$ | Constant numbers |
| $a, b, m, n, \mu_1, \mu_2, m_1, v_2$ | Mean stress sensitivity factor |
| M | Liu–Zenner equivalent stress |
| σ_{LZ} | Fatigue strength value for alternating axial loading |
| σ_w | Fatigue strength value for pulsating axial loading |
| $\sigma_{w(R=0)}$ | Fatigue strength value for alternating torsional loading |
| τ_w | Fatigue strength value for pulsating torsional loading |

1. Introduction

Structural components, such as engine and transmission parts, which experience more than around 10⁴ load reversals, could fail in service by High Cycle Fatigue (HCF). Such components can be designed to avoid failure by HCF if the applied stresses are kept below the metals fatigue strength. If the combined loads vary, relatively, in phase, amplitude and frequency, the prediction of the required metal fatigue strength is non-trivial and the accuracy of the prediction depends greatly on the nature of the multi-axial fatigue strength criterion used.

Crank drive shafts, pressure vessels, blade/rotor junctions, bolted junctions and many aeronautical components are usually operating under combined loads which can still be out of phase and in different frequencies generating complex biaxial or tri-axial states of stresses. The fatigue process under such states of stresses is known as Multi-axial Fatigue whose consideration is of fundamental importance for assessment of life and operational reliability of structural components. Therefore, efficient and accurate methodologies for the evaluation of fatigue endurance limit under multi-axial stress states are required for use in engineering design applications.

The initial theories proposed to predict fatigue failure under combined loading were basically an extension of the failure theories for static multi-axial state of stress to multi-axial states of cyclic stresses. The aim of these theories was to produce an uni-axial stress amplitude equivalent to a given multi-axial cyclic stress state and then use it to predict fatigue life from S-N curves, obtained from conventional fatigue tests. The Maximum Shearing Stress Theory of Fatigue Failure and the Distortion Energy Multi-axial Theory of Fatigue Failure were basically extensions of the Tresca and Von-Mises theories, respectively. The stress amplitudes were substitutes for the static principal stresses and the reversed fatigue strength or fatigue limit replaced the yield stress. The experimental evidence showed these methods were very conservative.

In the present study, Computer Aided Optimization (CAO) is used as an optimization method to improve the fatigue strength of notched components. The present approach is composed of five steps. Roughly speaking, it is based on associating the stress field in the notch zone, namely the "Growth Zone", with a temperature variation, and simultaneously decreasing the elastic modulus in that zone. The commercial finite element (FE) software ABAQUS 6.10 is used to apply this method. In the original CAO method which was developed by Mattheck, the Von-Mises stress was the criterion adopted for calculating the stress concentration factors and also the stress which should be transformed into temperature variation. Instead, in this work the Liu-Zenner is the chosen criterion due to the fact that based on the literature the fatigue limit assessment obtained by this method in different types of loading is often reliable for the material considered in this work. Liu-Zenner is an integral criterion based on the average value of the shear and normal stress acting on each material plane; thus an appropriate definition of shear stress on each plane is required. In this paper, the Papadopoulos definition of amplitude and a mean value of the shear stress acting on the plane is used. This definition is almost free from the ambiguities affecting other definitions, mainly regarding the uniqueness of the mean shear value, because it is based on the construction of a unique minimum-circumscribed circle to the load path described by shear stress on a given material plane. As mentioned earlier, in order to apply the Liu-Zenner criterion, it is necessary to calculate some integrals containing the expressions of the mean and the average stresses acting over all material planes. Actually, for numerical calculation, material planes orientation is varied in a step wise manner, in order to span all possible orientations. In this regard, the implementation of this procedure follows the Weber method and employs the algorithm for determination of the smallest circle surrounding the loading path proposed in the same reference. Finally, one example of automobile crankshaft based on the developed method is presented. Results obtained from the numerical examples indicate that

distribution of the Liu–Zenner equivalent stress over the notch area is significantly smoothed, in comparison with the original shapes, leading to decrease and, in some cases, even to the complete removal of any stress concentration at the notch. It has to be mentioned that the results have not been experimentally evaluated and the presented examples concern only the numerical improvement in the CAO method.

2. Optimization procedure

As we saw it before, by today there are many optimization procedure for component experiencing multi-axial loads are available. As fatigue failure is sudden and occurring in many components, many researchers are proposing new methods. Out of these methods we will discuss few of them here in this paper. We will also discuss about the chosen criterion Liu- Zenner procedure and our developed method.

The fatigue limit evaluation is substantially simplified when compared to the finite live estimation. Only the following condition is checked:

$$L.H.S.(load) = a \cdot f(C) + b \cdot g(N) \leq f_{-1} = R.H.S (material)$$

In the multi-axial fatigue analysis, the most often solution evaluates the load effects on selected planes, which are decomposed to shear stress C and normal stress N . The damage parameter formed on the left hand side is thus compared to the $f-1$ fatigue limit under reversed push-pull loading. If the inequality is fulfilled the loading is lower than the fatigue limit and the specimen will not break. For experimentally set fatigue limits, the relative evaluation of the condition leading to the FI fatigue index definition:

$$FI = L.H.S.(load) / R.H.S.(material)$$

should be equal to unity, i.e. both sides should be equal. Fatigue index greater than 1 computed for such fatigue limit experiments mean that the criterion is over-conservative (safe) and values lower designate un-safe prediction.

Below given are the different criterions used for multi-axial fatigue analysis:

Critical plane analyses (CPA) – different planes at the evaluated point are examined to find which provides the maximum value of the decisive variable. The methods can be further categorized accordingly:

1) The MSSR (maximum shear stress range) method searches for the plane with the maximum shear stress range, which is the critical plane.

2) The MD (maximum damage) method searches for the plane with the maximum damage parameter (L.H.S. in (2)).

3) The CPD (critical plane deviation) method - searches first for a fracture plane defined by some assumption, and then the critical plane is looked for with some specific inclination from the critical plane, while the damage parameter is maximized.

Integral analysis (IA) - the damage parameter or its individual components are integrated over all planes at the examined point

Ilyushin deviatoric space analysis (IDSA) - the criteria are mostly based on an analysis of an envelope of the load path analyzed in five dimensional Ilyushin deviatoric space.

In all cases where decomposition of the shear stress during the loading cycle is necessary, the method of the minimum circumscribed circle, as described by Papadopoulos in, is used in the incremental solution proposed by Bernasconi.

2.1 Available methods

There are many available methods for solution of multi-axial fatigue loading. Here we have discussed only few and important of them.

Matake (MAT)

A frequently cited criterion with a linear combination of shear stress amplitude and maximum normal stress is by Matake, and is defined in a maximum shear stress range (MSSR) variant. The groups of experiments evaluated by mean DFI values can nevertheless provide some material for an evaluation. Uniaxial load cases with mean loads tend to lead to non-conservative predictions. There is also an important difference between the groups with axial + torsion and axial + axial load combinations. The suspicion is mentioned for the Susmel criterion, below, that the MSSR

concept is not the right solution for out-of-phase loading. The Findley method uses the same damage parameter but prefers the maximum damage scheme. Because it provides better results, no reason was found for improvements to the Mataka method.

Sines (SIN)

The Sines criterion is one of the oldest and best-known criteria. The Sines criterion results show that its frequent use in various comparisons should be abandoned (similarly to the Mataka criterion). The mean stress effect realized only through the mean hydrostatic stress is not adequate, and for pure torsion and pure axial load cases it results in a distinct shift in the opposite directions from the ideal prediction. The Sines criterion also provides non-conservative predictions for brittle materials. The formulation of the Sines criterion is very close to the Crossland method and only the mean stress effect incorporation differs. Because the results of the Crossland method show much better prediction quality, no further elaboration of the Sines method can be recommended.

Findley (FIN)

The Findley damage parameter is the same as Mataka's, but the critical plane concept is based on the search for the maximum damage assumption. Although its results are substantially better than those provided by the Mataka criterion, the range and standard deviation remain unsuitably high. Positive factors are that the out-of-phase loading is well mastered. A revision of the mean stress effect could substantially improve the predictive quality of this criterion.

Susmel (SUS)

The criterion published by Susmel and Lazzarin is based on the idea of including the critical plane stress ratio:

$$\rho = \frac{N_{max}}{C_a}$$

in the basic formula to relate the shear and normal stress effects.

This interesting idea leaves the dimension of the second load term in the damage parameter one order lower than for the shear parameter, similarly to the Papuga PCr criterion. The critical plane criterion is of the maximum shear stress range (MSSR) type.

An improved version was formulated by Susmel himself by revising the ρ ratio:

$$\rho = \frac{Na + d_{Su}.Nm}{Ca}$$

Susmel does not state in how to set the dSu parameter. His only commentary concerns its expected range (0; 1) and a proposal for its value for various tested materials, which cannot be accepted as a general approach.

Papadopoulos (PAP)

It was Papadopoulos who started the trend of the comparative analysis of different criteria in the 1990s. Papadopoulos also provided a simple analytical formula of his criterion valid for the axial + torsion load case, and thus his criterion is widely cited and evaluated in many research papers. In addition to the common integration over all planes necessary for all criteria using an integral approach, another level of integration of the resolved shear stress over the shear plane has to be performed, which seems to prevent the criterion from being applied in commercial fatigue solvers, due to its high demand on a computation time.

In his paper, Papadopoulos recommends that his criterion be applied above all for materials in the range (1.25; 1.73) of k , i.e. for metals with ductile characteristics. The results provided for brittle or extra-ductile materials are slightly shifted by the mean DFI value from the mean DFI value of the group with ductile materials, but the differences are not very distinct. A problem of greater importance is the trend toward non-conservative prediction achieved for many of the load cases, even

simple uniaxial cases, with mean stress involved. The weak mean stress effect caused by the inclusion of maximum hydrostatic stress is not the only negative aspect of the criterion.

Crossland (CRO)

The same combination of the amplitude of the second invariant of the stress tensor deviator and the hydrostatic stress as by Sines differs in the incorporation of the mean stress. While Sines proposes the use of the mean hydrostatic stress, Crossland prefers its maximum value. The difference has a tremendous effect on the prediction results. The Crossland criterion has a good DFI range parameter, but there is also a shift to the non-conservative side and there are very high scatters. When the individual groups of tests are evaluated in there is a pronounced shift of the out-of-phase load cases to the non-conservative side. This finding, indicates that though the Crossland criterion incorporates the mean stress very well, its applicability to out-of phase loading is poor.

Papuga PCr (PCR)

Criterion was introduced in full detail by Papuga and Ruzicka. It uses the hybrid combination of shear stress amplitude quadrature and linear normal stress amplitude and the mean stress effect is proposed as the best fit to the available experimental data.

The criterion is the only one that nearly gets to a fatigue index error in the range (-20; 20)%. However, it is understood from a more detailed search for some negative properties that its behaviour under the torsion mean load is not perfect because of the shift of the results to the non-conservative side.

2.2 Liu–Zenner criterion

Among different criterions Liu-Zenner is chosen criterion for this study. It is explained in detail here.

The Liu–Zenner criterion has been chosen in order to optimize the notched shapes. Although this criterion requires a complicated numerical approach, it needs four different material properties, and it is limited to a range of materials. Its use for the material which has been considered in the study example has been justified by the good agreement of predictions with some experimental tests. Moreover, based on the literature, the estimated fatigue predictions according to this criterion show appropriate results in different loading conditions.

The criterion is based on Eqs. (1)–(3), with reference to the schematic diagram of Figure 2.1. In the following equations the $\sigma_{va,\tau}$ and $\sigma_{va,\sigma}$ stress amplitudes, are calculated using the following integrals at each time step as function of the stress components.

$$\sigma_{va,\tau} = \left\{ \frac{15}{8\pi} \int_{\gamma=0}^{\pi} \int_{\varphi=0}^{2\pi} \tau_{\gamma\varphi a}^{\mu_1} \text{Sin}\gamma d\varphi d\gamma \right\}^{1/\mu_1} \quad (1)$$

$$\sigma_{va,\sigma} = \left\{ \frac{15}{8\pi} \int_{\gamma=0}^{\pi} \int_{\varphi=0}^{2\pi} \tau_{\gamma\varphi a}^{\mu_2} \text{Sin}\gamma d\varphi d\gamma \right\}^{1/\mu_2} \quad (2)$$

$$\sigma_{va} = \left[a\sigma_{va,\tau}^2 + b\sigma_{va,\sigma}^2 \right]^{1/2} \quad (3)$$

$$a = \frac{1}{5} \left[3 \left(\frac{\sigma_W}{\tau_W} \right)^2 - 4 \right], b = \frac{1}{5} \left[6 - 2 \left(\frac{\sigma_W}{\tau_W} \right)^2 \right]$$

In these equations the exponent's μ_1 and μ_2 can be varied between 2 and infinity. In order to simplify the calculation, the exponents are often selected as

$\mu_1 = \mu_2 = 2$. The coefficients a and b are determined for pure alternating tension–compression and pure alternating torsion.

This equation should be valid only for $a, b > 0$. Therefore, this method, with $\mu_1 = \mu_2 = 2$, is only applicable for the materials fulfilling the requirements expressed by the following inequalities:

$$\frac{2}{\sqrt{3}} \leq \left(\frac{\sigma_w}{\tau_w} \right) \leq \sqrt{3} \quad (4)$$

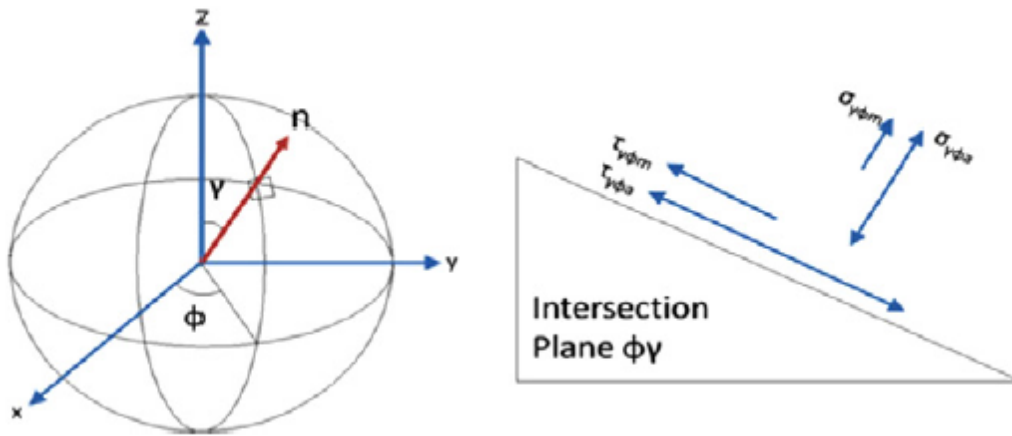


Figure 2.1 Integration domain of the SIH and stress components in the intersection plane $\gamma\phi$.

The equivalent mean stresses, and the mean normal stresses are calculated as follows by considering $v_1 = v_2 = 2$:

$$\sigma_{vm,\tau} = \left\{ \frac{\int_{\gamma=0}^{\pi} \int_{\phi=0}^{2\pi} \tau_{\gamma\phi a}^{\mu_1} \tau_{\gamma\phi m}^{v_1} \text{Sin}\gamma d\phi d\gamma}{\int_{\gamma=0}^{\pi} \int_{\phi=0}^{2\pi} \tau_{\gamma\phi a}^{\mu_1} \text{Sin}\gamma d\phi d\gamma} \right\}^{1/v_1} \quad (5)$$

$$\sigma_{vm,\sigma} = \left\{ \frac{\int_{\gamma=0}^{\pi} \int_{\phi=0}^{2\pi} \tau_{\gamma\phi a}^{\mu_2} \tau_{\gamma\phi m}^{v_2} \text{Sin}\gamma d\phi d\gamma}{\int_{\gamma=0}^{\pi} \int_{\phi=0}^{2\pi} \tau_{\gamma\phi a}^{\mu_2} \text{Sin}\gamma d\phi d\gamma} \right\}^{1/v_2} \quad (6)$$

And finally, the failure condition is formulated directly by a combination of all the equivalent stresses from Eqs. (3), (5), and (6), resulting into:

$$\sigma_{va}^2 + m\sigma_{vm,\tau}^2 + n\sigma_{vm,\sigma}^2 = \sigma_W^2 \quad (7)$$

$$m = \frac{\sigma_W^2 - \left(\frac{\sigma_W}{\tau_W}\right)^2 \left(\frac{\tau_{W(R=0)}}{2}\right)^2}{\frac{4}{7} \left(\frac{\tau_{W(R=0)}}{2}\right)^2},$$

$$n = \frac{\sigma_W^2 - \left(\frac{\sigma_{W(R=0)}}{2}\right)^2 - \frac{4m}{21} \left(\frac{\sigma_{W(R=0)}}{2}\right)^2}{\frac{5}{7} \left(\frac{\sigma_{W(R=0)}}{2}\right)^2} \quad (8)$$

For calculating the equivalent stress, the values of the fatigue limit for pure bending σ_W , the fatigue limit for pure torsion loading τ_W and the fatigue limit for alternating bending and torsion, $\sigma_{W(R=0)}$, $\tau_{W(R=0)}$ respectively, are required. The fatigue limit under pulsating tensile stresses $\sigma_{W(R=0)}$ is evaluated by assuming a linear relationship between the allowable stress amplitude σ_W and the stress ratio R, introducing a mean stress sensitivity factor M, whose expression is

$$M = \frac{\sigma_W - \sigma_{W(R=0)}}{\sigma_{W(R=0)}} = 0.2 \quad (9)$$

The value of M is material dependent, and a linear relationship with tensile strength of the material was proposed. Accordingly, the value of M has been set to 0.2. For the fatigue limit under pulsating torsion stress the same assumption as in is made, resulting into the expression

$$\tau_{W(R=0)} = \frac{4\tau_W}{1 + \frac{2\sigma_W}{\sigma_{W(R=0)}}} \quad (10)$$

Definition of shear stress amplitude and mean value:

In the integral type approaches the correct definition of the shear stress amplitude and mean value, constitutes the most crucial task. Evaluation of amplitude and mean value of the shear stress acting on the critical plane can be easily resolved for proportional cyclic loading conditions. The situation is much more complex regarding the definition of amplitude and mean value of the shear stress for non-proportional loading. The complexities arise from the fact that, unlike the normal stress vector which conserves its direction, the shear stress vector s

changes in magnitude and direction inside each load cycle. The minimum-circumscribed circle (MCC) to the path described by the tip of the shear vector on the material plane under consideration allows defining a unique set of shear stress amplitude and mean shear stress values. If the stress-time history is defined over a finite number of time steps, the load path becomes a polygon. The MCC circumscribing a plane polygon P is: either one of the circles drawn with a diameter equal to a line segment joining any two vertices of P or one of the circum circles of all the triangles generated from every three vertices of P. Thus in principle the MCC could be found by examining all these possible circles. This method was presented for the first time by Papadopoulos; however it has been proven that other methods exist to find MMC with better computational efficiency. In this study a new method, the Mean Point method, is presented.

The mean point method

The most important implication of the proposed definition of the amplitude and the mean value of the shear stress is the implementation of a practical and accurate mathematical way to find the minimum circumscribe circle (MCC) for a given set of points. There are many different geometrical algorithms such as the longest chord method, the longest projection method, the minimum-circumscribed circle method, etc. And there are also some numerical ways to find this circle such as the points combination algorithms, the incremental algorithm, Optimization algorithms, Randomized algorithms, etc. The method which is applied in this paper is a mixed implementation of the randomized algorithms, the longest chord method, and the modified Weber method for the point's combination algorithms. They proposed one such modification in order to reduce the calculation duration of the critical plane approach in fatigue. Due to the fact that this method is started with finding the mean point which is somehow like the centre of gravity of the given set of points, it is named the mean point method. The algorithm of this method is as follows:

1- For the set of n point P_i find the mean point A which is

$$x_A = \frac{\sum x_{p_i}}{n} , \quad y_A = \frac{\sum y_{p_i}}{n}$$

2- Find the points Q_i which have the longest distance R of A

3- If set Q consists more than two different points the circle with these point is MCC

4- If set Q consists only two different points:

- a. If A and these two points are in a line the circle with the centre of A and one of these point is MCC
- b. Otherwise from now on we know that the researched MCC has at least three points in common with P and two of them are in Q for fining the third one the easiest way is to check the entire possible circles which are $n-2$. The MCC should be consists all of set point P and also the radius of it must be smaller than R .

5- If there is only one point which has the longest distance of A based on the randomized method this point should be on the on the boundary because it is possible to draw a circle with the centre of A and the radius $R-\epsilon$ which consists all the points except for Q ; therefore the MCC which should contain all the point will be a circle with Q on the boundary. At the moment, the circle with the centre of A and radius R is named MCC. Because MCC must be a circle with two points on the boundary or three points, we should follow two others following steps:

- a. Based on the longest chord method, find the point P_1 which has the longest distance from Q . If this circle with centre A_0 contains all the points of P and also the radius is smaller than R . Replace this circle with MCC. For all likelihood, this circle is MCC but for being sure it seems necessary to continue to the next stage.
- b. In this step, all the possible circles with three points should be checked. But it needs $\binom{P-1}{2}$ calculation to find

the different circles. In order to reduce the number of iteration the modified Weber method is used. Based on this method, we start with the circle in previous step. Whether it was MCC or not. Based on the modified Weber method, the MCC will be found with the farthest point from the centre of the previous circle. More information is available in.

6- After step 5 the smallest circle which contains all the point is MCC. The advantage of this method is finding the Q point which is for sure is on the boundary. This finding considerably reduces the number of iterations.

2.3 Optimization procedure

The original CAO technique considers the Von-Mises stress as the quantity with respect to which the optimization is performed; thus the procedure will lead to modification of the original geometry in such a way that the maximum Von-Mises stress is reduced. If a structural element is subjected to multi-axial fatigue loading, the Von-Mises stress can no more be used as a reference parameter for notch optimization, particularly in the case of out-of-phase loading. Thus, the original CAO technique is modified to be applied to general multi-axial fatigue loadings. The modified CAO method is briefly described in the following steps. The flowchart is also illustrated in Figure 2.2.

1. A FE model of the structure representing the actual appearance of the component is produced by ABAQUS 6.10. Fatigue loading is applied by introducing the stress amplitude and the relative phases of the harmonic function expressing the variation of stress components with time; thus, the history of stress tensor through the time is assigned to each node with a limitation to harmonic loadings.

2. Based on the FE results the Liu-Zenner equivalent stress at each node will be calculated by using a subroutine written in Python 2.4. The strength of the structure could be estimated based on comparison of the calculated equivalent stress with the fatigue limit of the material.

3. The computed stresses are then substituted by a virtual temperature distribution. In this way the points which previously showed the highest mechanical stresses would be the hottest points in the component. Moreover, the modulus of elasticity in the highly stressed layer is set to only 1/400 of the initial value. Thus there would be a fictitious soft layer with particularly high temperature at the original overloaded zones and rather cold layers in the unloaded regions. The important point is defining the initial temperature, it is necessary to

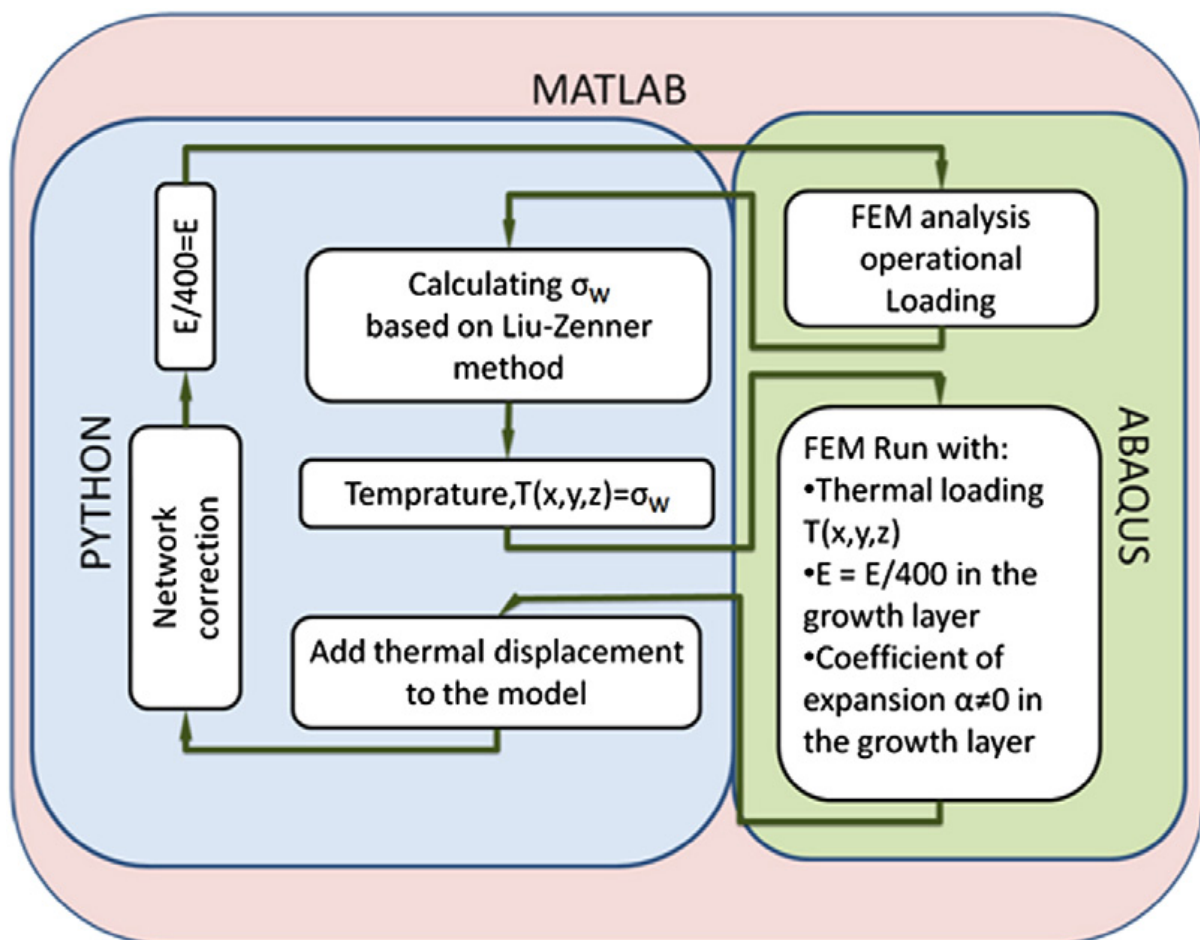


Figure 2.2. Flowchart of the Modified CAO method

define an appropriate initial value with reference to the stress values. In this regard, the mean value of the stresses in the Growth Zone has been chosen as an initial value for the temperature.

4. In the next FE computation only the previously determined thermal loads are applied, whereas the previously applied mechanical

loads are set to zero. Moreover, only the soft, heated layer will have a thermal expansion factor $\alpha > 0$. During this computational stage with only thermal loading applied, the 'pudding-soft' layer expands corresponding to its temperature distribution. That is the Growth Zone which previously experienced the highest loads (in computation step 2), at this stage is subjected to the highest temperature variations and consequently expands more. This step of the procedure is controlled by a Matlab 2007 subroutine.

5. The structure, already improved by growing in computation step 4, is already shape-optimized to some extents, and occasionally one such growth cycle is sufficient. This is checked by setting again the E-modulus of the soft layer at the value of the basic material and starting from step 2 with a new FE computation under purely mechanical loading, which will deliver a more homogeneous stress distribution with greatly reduced notch stresses. The computation loops 2–5 are run through repeatedly, till the stress concentration factor stops changing within a given tolerance or due to the fact that construction conditions forbid further growth.

3. Application of modified CAO

In this study we have considered automobile crankshaft as our component for shape modification.

In the working cycle, crankshaft experiences bending and torsional loads due to reciprocating motion of connecting rod. The main objective was the optimization of the shape of fillets on the forged steel crankshaft (which causes high stress concentration and ultimately fatigue failure) which requires accurate magnitude of the loading on this component that consists of bending and torsion. It is needed to check variation of both loads throughout the working cycle.

It is very important to find out loads coming on the crankshaft throughout the working cycle. There is an analytical approach to find out the loads on the crankshaft. MATLAB can be used to find out these stresses. In this project, we have used already available results of loads taken from a paper published by Ali Fatemi (2007).

ADAMS software can be used for analytical approach also.

3.1 Dynamic Load analysis

For analytical approach, they generally use slider-crank mechanism with a single degree of freedom. The figure 3.1 shows slider-crank mechanism used for analytical approach. θ is the degree of freedom.

MATLAB is used to solve nonlinear equations of this slider crank mechanism.

3D dynamic analysis can be done using ADAMS. For 3D analysis, material density of 2840 kg/m^3 was used. Speed of crankshaft as 3600 rpm was considered. 3600 rpm is the maximum operating speed of engine. It is mentioned in Ali Fatemi's paper that the engine speed effect within the operating engine speed of 2000 rpm to 3600 rpm, is less than 15% on the force range applied to the crankshaft. The 3D model used in ADAMS is shown in figure 3.2. Table 3.1 shows details of the slider crank mechanism used. As we have taken all results from Ali Fatemi's paper, we

are not discussing about the procedure. These results are for four stroke engine so a cycle completes after 720 degrees.

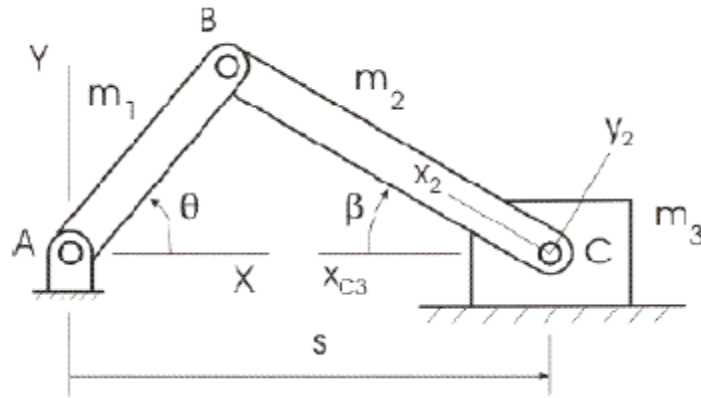


Figure 3.1. Slider crank mechanism

| | Crank AB | Connecting rod BC | Slider C |
|--------------------------------|----------|-------------------|-----------|
| Calculated Mass (kg) | 3.7191 | 283.35E-3 | 417.63E-3 |
| I_{xx} (kg-mm ²) | - | 608.5844 | - |
| I_{yy} (kg-mm ²) | - | 80.3227 | - |
| I_{zz} (kg-mm ²) | - | 662.5235 | - |
| I_{xy} (kg-mm ²) | - | 8.0467 | - |
| I_{xz} (kg-mm ²) | - | 0 | - |
| I_{yz} (kg-mm ²) | - | 0 | - |
| Length (mm) | 36.985 | 120.78 | - |

Table 3.1. Details of slider crank mechanism used in ADAMS

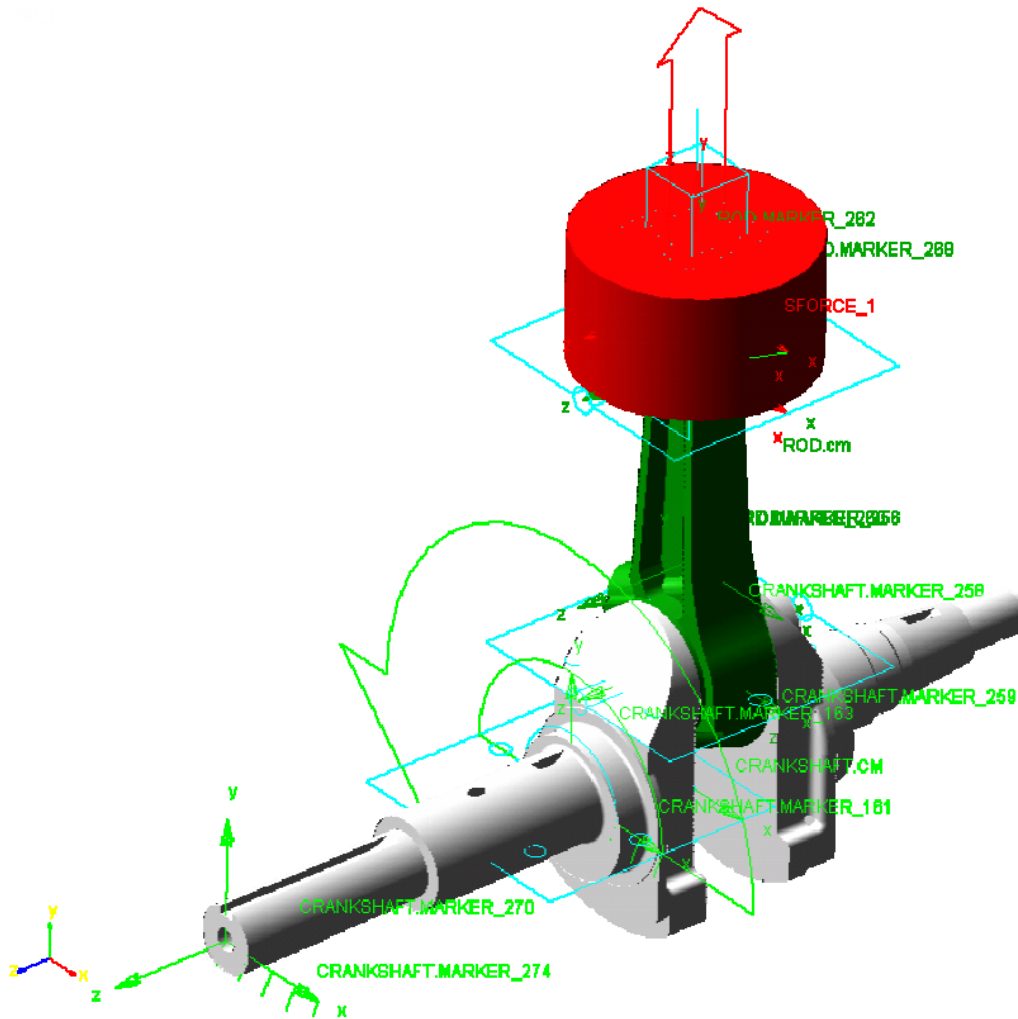


Figure 3.2 Slider crank mechanism used in ADAMS

This was an analytical way to find out forces on the crankshaft during its working cycle. In actual we have used pressure volume graph for 720 degree cycle. Table 3.2 shows the configuration of the engine to which this forged crankshaft belongs. Figure 3.3 shows the pressure volume graph and figure 3.4 shows the pressure versus crankshaft angle graph. The pressure versus volume of the cylinder graph changes as a function of engine speed, but the changes are not significant and the maximum pressure which is the critical loading situation does not change. We have considered maximum operating speed as 3600 rpm.

| | |
|--|---------------------------------------|
| Crankshaft radius | 37 mm |
| Piston diameter | 89 mm |
| Mass of the connecting rod | 0.283 kg |
| Mass of the piston assembly | 0.417 kg |
| Connecting rod length | 120.78 mm |
| I_{zz} of connecting rod about the center of gravity | $0.663 \times 10^{-3} \text{ kg-m}^2$ |
| Distance of C.G. of connecting rod from crank end center | 28.6 mm |
| Maximum gas pressure | 35 Bar |

Table 3.2 Configuration of Engine

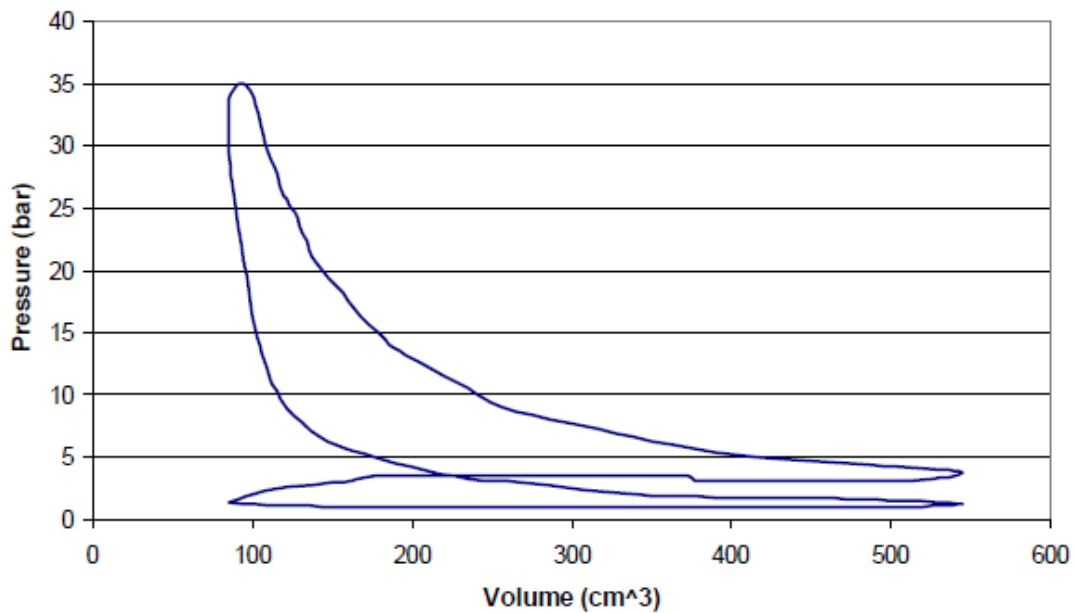


Figure 3.3. Pressure versus volume diagram

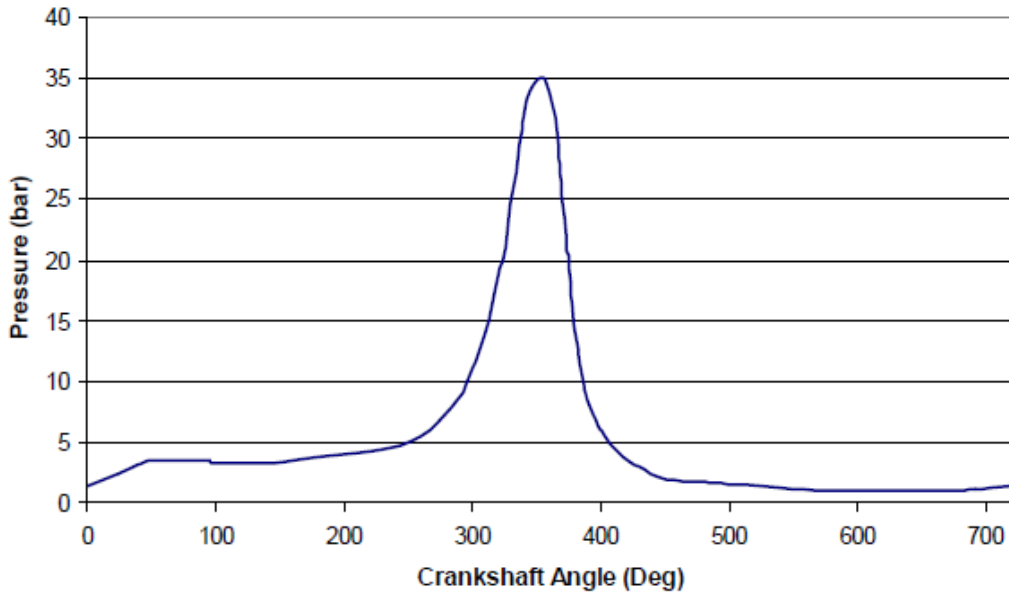


Figure 3.4 Pressure versus crankshaft angle through one cycle.

Figure 3.5 shows the force versus angle diagram. F_x is the force that causes bending and F_y is the force that causes torsion on the crankshaft. The maximum loading happens at the angle of 355° where the combustion takes place.

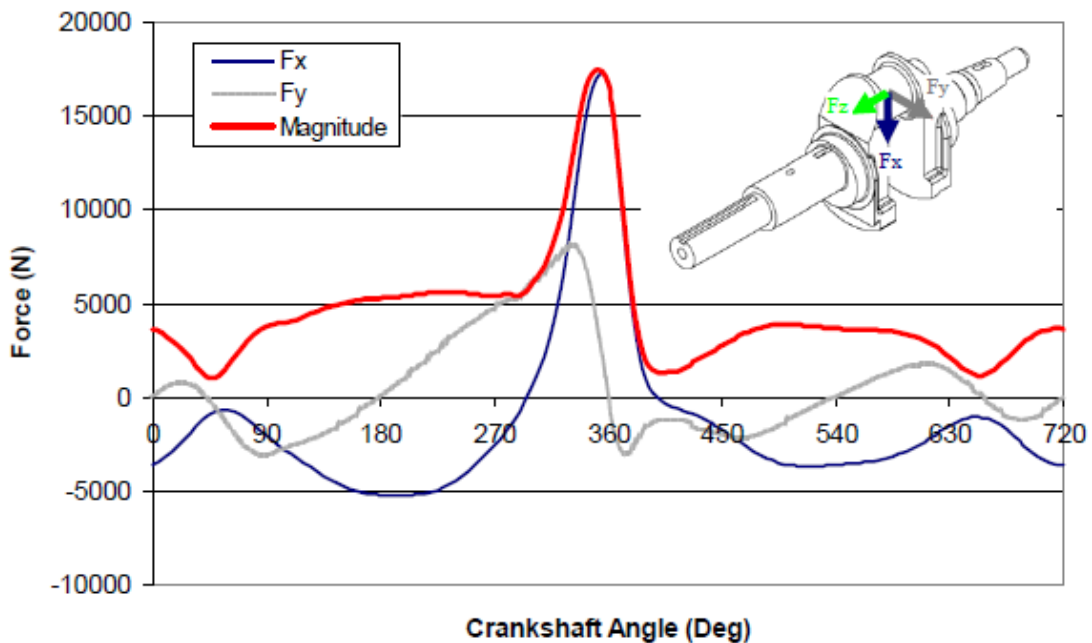


Figure 3.5 Force versus crankshaft angle during 720 degrees for an engine having 3600 rpm.

It is known that as the engine speed increases the maximum bending load decreases. Combustion and inertia are two load sources in the engine. The maximum pressure in the cylinder does not change as the engine speed changes; therefore the load applied to the crankshaft at the moment of maximum pressure due to combustion does not change. This is a bending load. The inertia load varies as a function of engine speed. As the engine speed increases this force increases too. The bending load due to combustion is greater than the inertia load and is in the opposite direction that means the sum of these two forces results in the bending force at the time of combustion. So as the engine speed increases the magnitude of the inertia force increases and this amount is deducted from the greater force which is caused by combustion, resulting in a decrease in total load magnitude.

The torsional load has no effect on the range of von Mises stress at the critical location. The reason behind it is that the maximums of bending and torsional loading happen at different times during the engine cycle. Also at the main peak of the bending the magnitude of torsional load is zero.

In a multi-cylinder crankshaft high torsional load must be included in the analysis because it is the effect of combustion of other cylinders on one cylinder.

3.2 Finite element modelling

To obtain the stress time history there are two different ways for applying the loads on the crankshaft. One method is to applying the magnitude of the load with its direction in a way that the loading could define the stress-time history of the component and to run the FE model many times during the engine cycle or at selected times over 720° . Another way is by superposition of the basic loading conditions. This involves applying a unit load in the basic conditions and then scaling the

stresses from each unit load according to the dynamic loading. Then similar stress components are added together.

In this study we have used first approach to make dynamic analysis of crankshaft and 3600 rpm is considered.

Locations for applying load are taken as 10 different points. We have considered following 10 different points:

- 1) at 0 degrees (Beginning of the cycle)
- 2) at 90 degrees
- 3) at 180 degrees (Valley of the bending load)
- 4) at 270 degrees (Bending load almost zero)
- 5) at 315 degrees (Peak of torsional load)
- 6) at 360 degrees (Actual pressure peak occurs at 355 degrees, but we have considered it at 360 degrees)
- 7) at 405 degrees (Bending load almost zero)
- 8) at 450 degrees (Valley of total load magnitude)
- 9) at 540 degrees (Selected to have smooth connectivity between the points before and after)
- 10) at 630 degrees

After analysing dynamic loading condition only two main loading conditions were applied to the surface of the crankpin bearing. These two loads are perpendicular to each other and their directions are shown in Figure 3.6 as F_x and F_y .

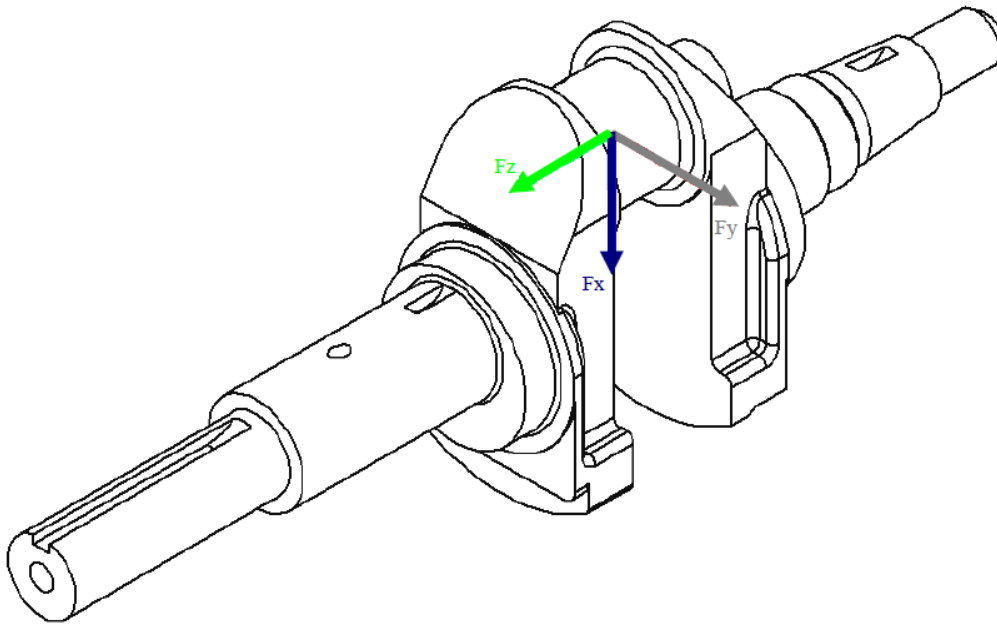


Figure 3.6 Three different loadings on crankshaft bending (F_x), torsional (F_y), and longitudinal (F_z).

3.2.1 Geometry generation

It is very important to generate accurate model for finite element analysis to get correct results. For finite element analysis we have used Abaqus. In Abaqus it is possible to generate simple geometry. As a complicated geometry, crankshaft is not generated in Abaqus. For geometry generation we have used Catia-V5. After generation of geometry it is imported to Abaqus.

Figure 3.7 shows the solid model of the forged steel crankshaft, and Figure 3.8 shows a picture actual forged crankshaft. Threaded front shaft is not threaded in the model, since this part does not carry any load and boundary conditions and has no effect on stresses. Another simplification made to forged steel crankshaft model was neglecting the slight slope on the crank web from outside toward centreline of main bearings. The slope is a result of manufacturing process. Slope is used for easy removal of part from the forging die. Since the change in the web thickness was

small, by averaging thickness over the entire crank web, the crank web was modelled with uniform thickness. This simplification is acceptable since stresses at this location are very low and the thickness does not change the results at the fillet areas, which are critical locations.

Drilled holes present on the counter weights are not considered in the modelled geometry as they do not affect on the stresses at critical locations.

The material properties used in is tabulated in the table 3.3.

Figure 3.9 shows dimensional drawing of forged crankshaft.

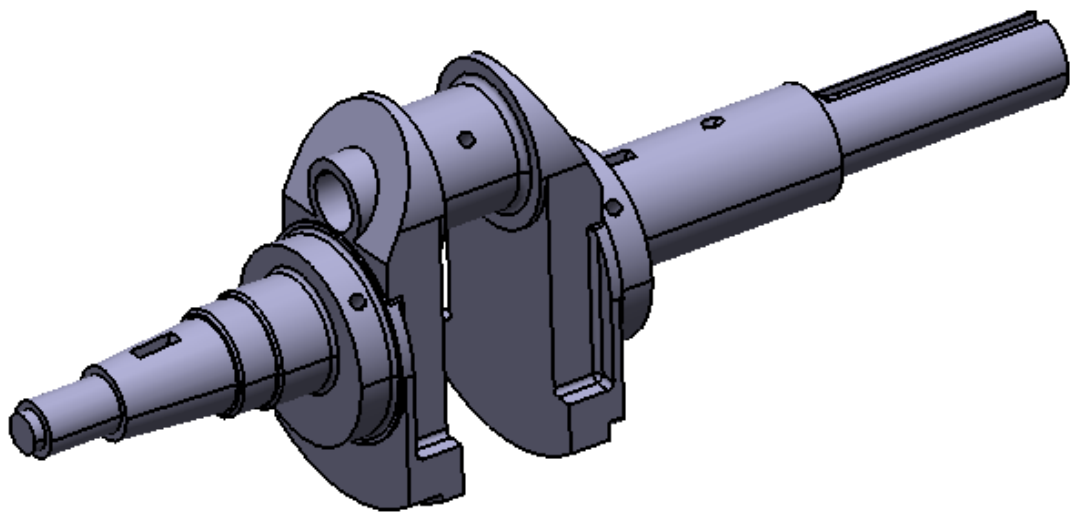


Figure 3.7 Solid model of Forged crankshaft generated in Catia-V5

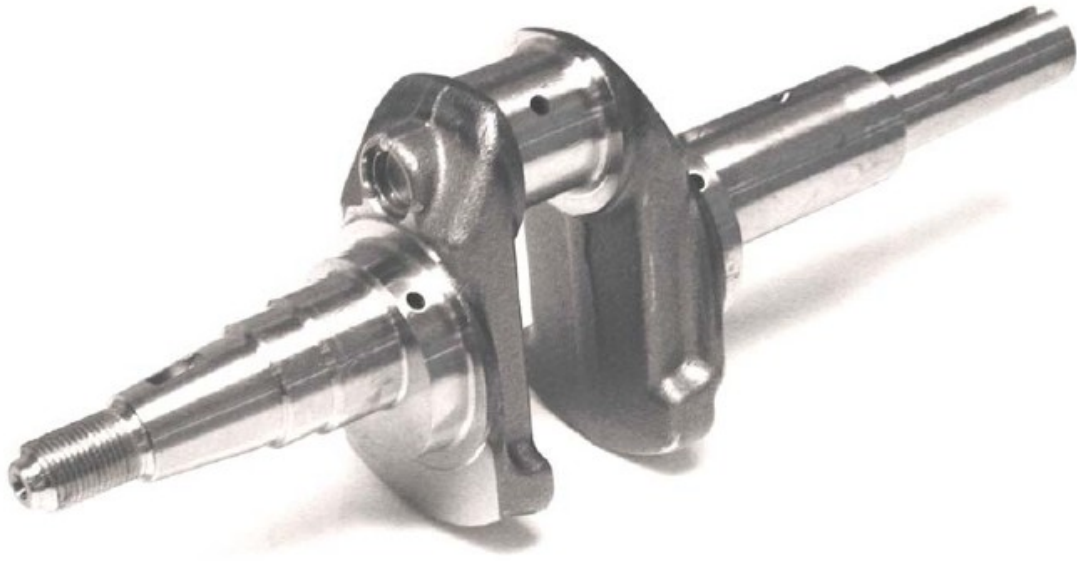


Figure 3.8 Actual picture of Forged steel Crankshaft

| Material Property | Unit | Forged Steel |
|-----------------------|-------------------------|--------------|
| Modulus Of Elasticity | <i>GPa</i> | 221 |
| Poisson's Ratio | - | 0.30 |
| Mass Density | <i>Kg/m³</i> | 7833 |

Table 3.3 Material Properties of forged crankshaft

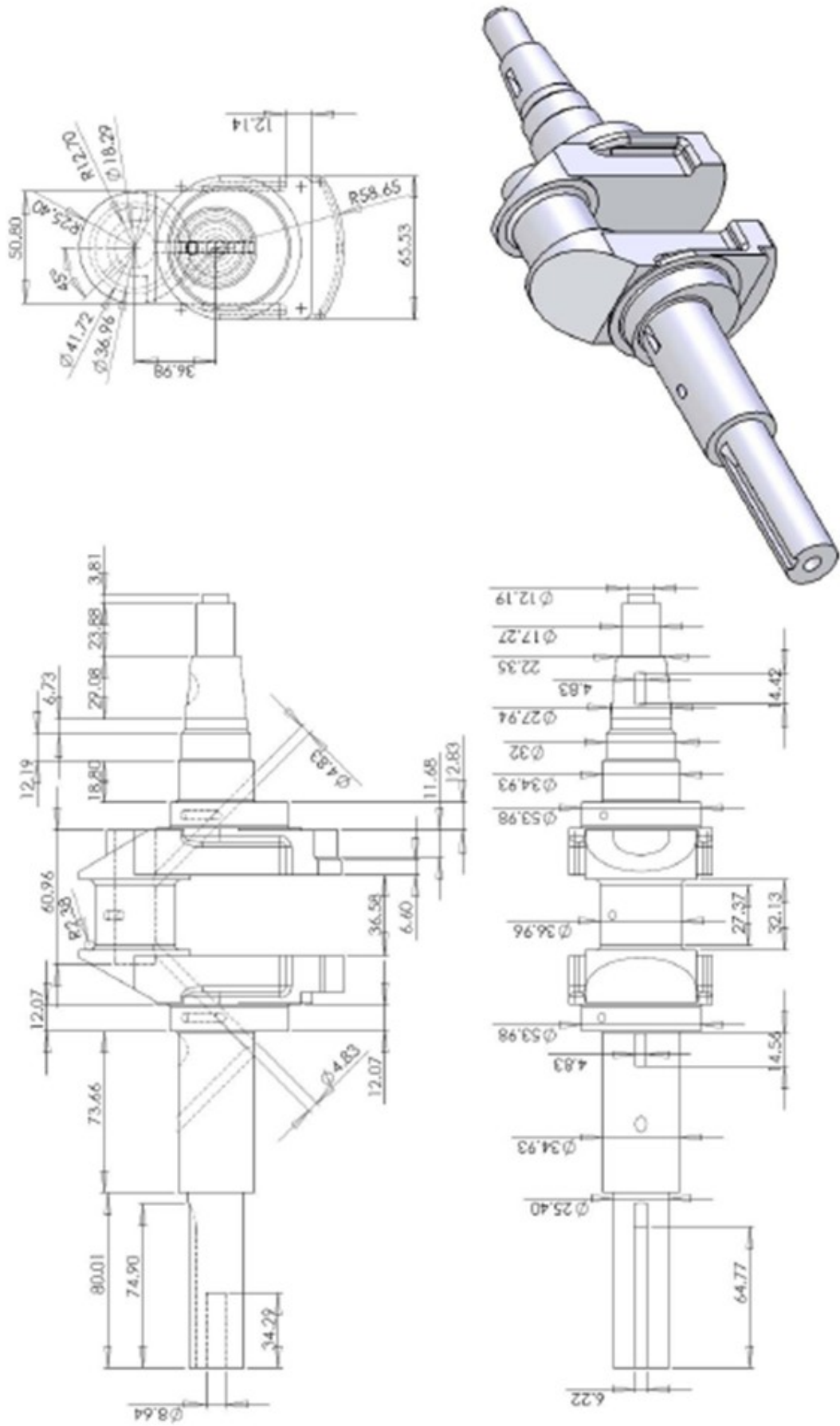
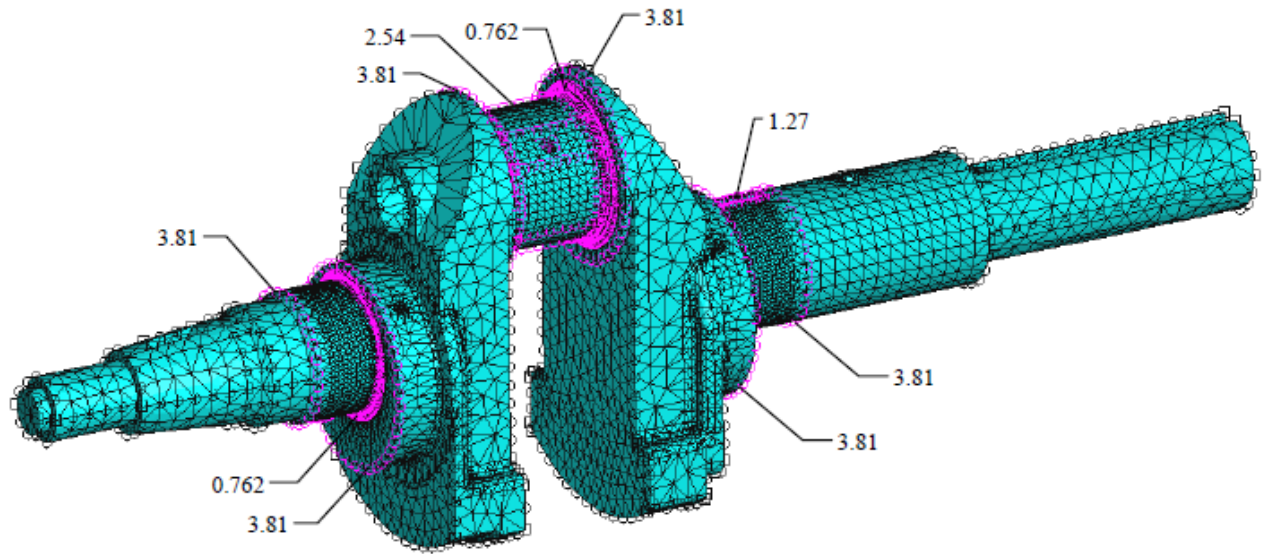


Figure 3.9 Dimensional drawing of forged crankshaft.

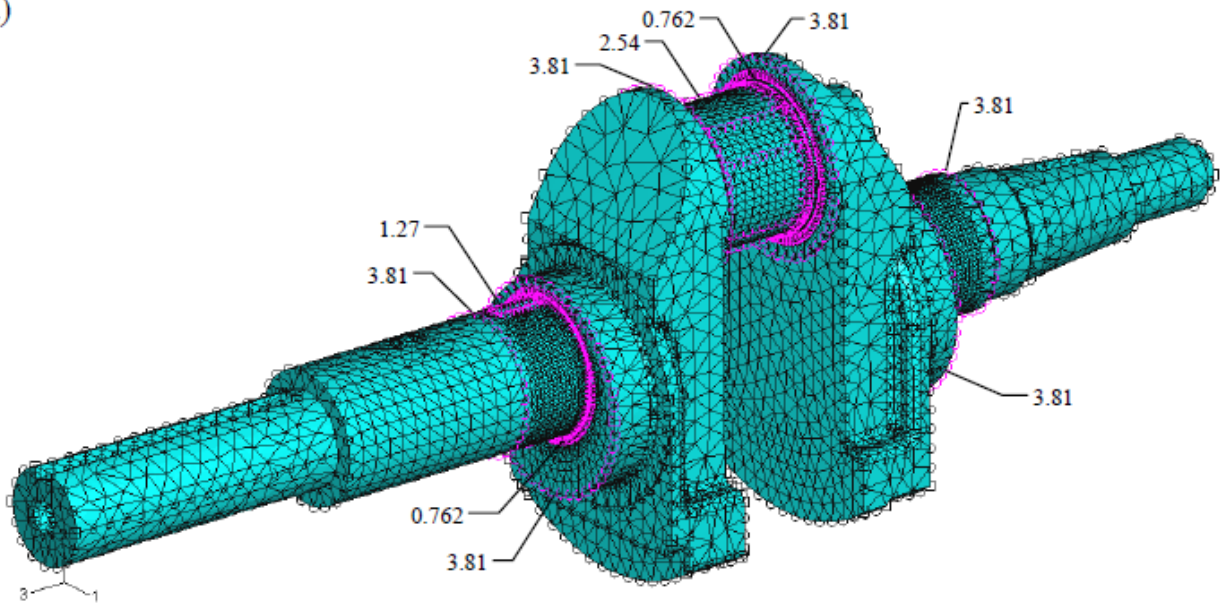
3.2.2 Mesh Generation

It is needed to mesh the geometry with quadratic tetrahedral elements for accurate results. But due some technical problem we have used linear tetrahedral elements for meshing. It will not change much in results. In abaqus tetrahedral elements are the only option for meshing the imported complex geometries. Using linear tetrahedral elements will result in a rigid model with less accuracy, whereas using quadratic tetrahedral elements will increase the accuracy and lessen the rigidity of the geometry. We used free meshing where we can define global size of elements. We can refine mesh at critical locations like the locations with higher gradient of stresses.

Convergence of stress at different locations was considered as the criterion for mesh size and number of elements selection. Satisfactory results were obtained at 258074 elements. We used global mesh size as 5 and local mesh size as 0.7. The selection of different sizes for elements was made to obtain a uniform growth of element size as the element size changed through the geometry. Figure 3.10 shows element sizes used at different locations for the forged steel crankshaft. Figure 3.11 shows the meshed geometry of forged crankshaft.



(a)



(b)

Figure 3.10 Element sizes used at different locations for the forged steel crankshaft. (a) and (b) are front and back views respectively.

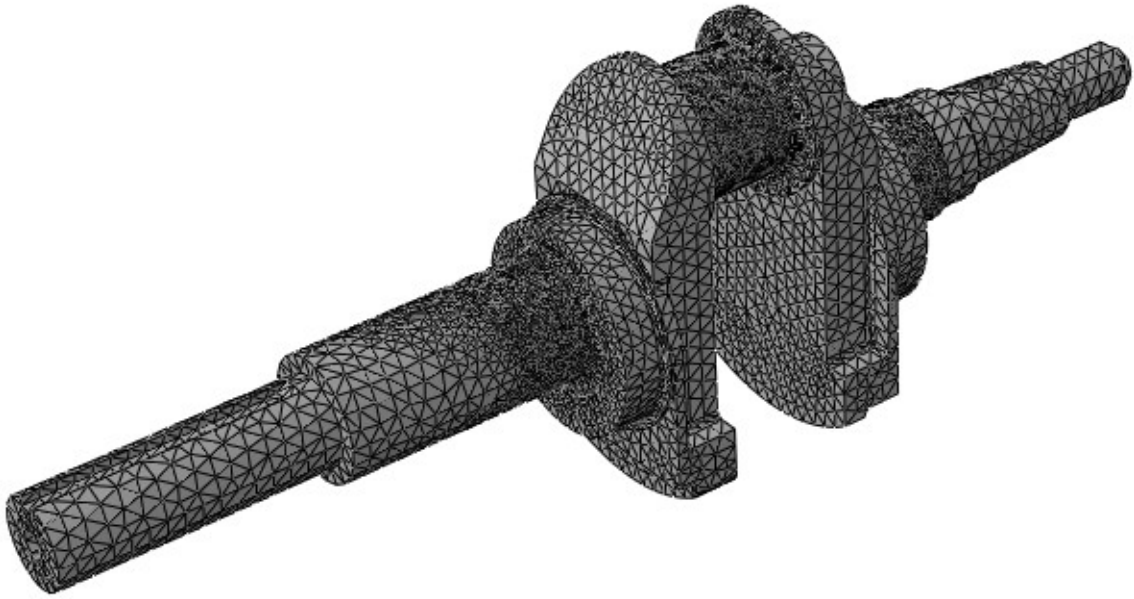


Figure 3.11 The meshed geometry of forged crankshaft.

3.2.3 Loading and Boundary conditions

Generally engine manual is used to find boundary conditions for the crankshafts. Figure 3.12 was taken from the engine manual of the forged steel crankshaft and shows different components at a cut view of the engine. It can be easily seen that the crankshaft is constrained with a ball bearing from one side and with a journal bearing on the other side. The ball bearing is press fit to the crankshaft and allows only the crankshaft rotation about its main central axis. Since only 180 degrees of the bearing surfaces facing the load direction constraint the motion of the crankshaft, this constraint was defined as a fixed semicircular surface as wide as the ball bearing width on the crankshaft. The other side of the crankshaft is on a journal bearing. Therefore, this side was modelled as a semicircular edge facing the load at the bottom of the fillet radius fixed in a plane perpendicular to the central axis and free to move along central axis

direction. Figures 3.12 show these defined boundary conditions in the FE model of forged steel. Boundary conditions rotate with the direction of the load applied such that the inner face of the fixed semicircular surface and sliding ring face the direction of the load. Definition of a fixed edge is based on the degrees of freedom in a journal bearing, which allows the crankshaft to have displacement along its central axis.

The load is applied at different angles. Load is applied as a concentrated load on the pin surface and at the centre of pin as shown in figure 3.13. Load is applied in two directions F_x and F_y , taken from figure 3.4.

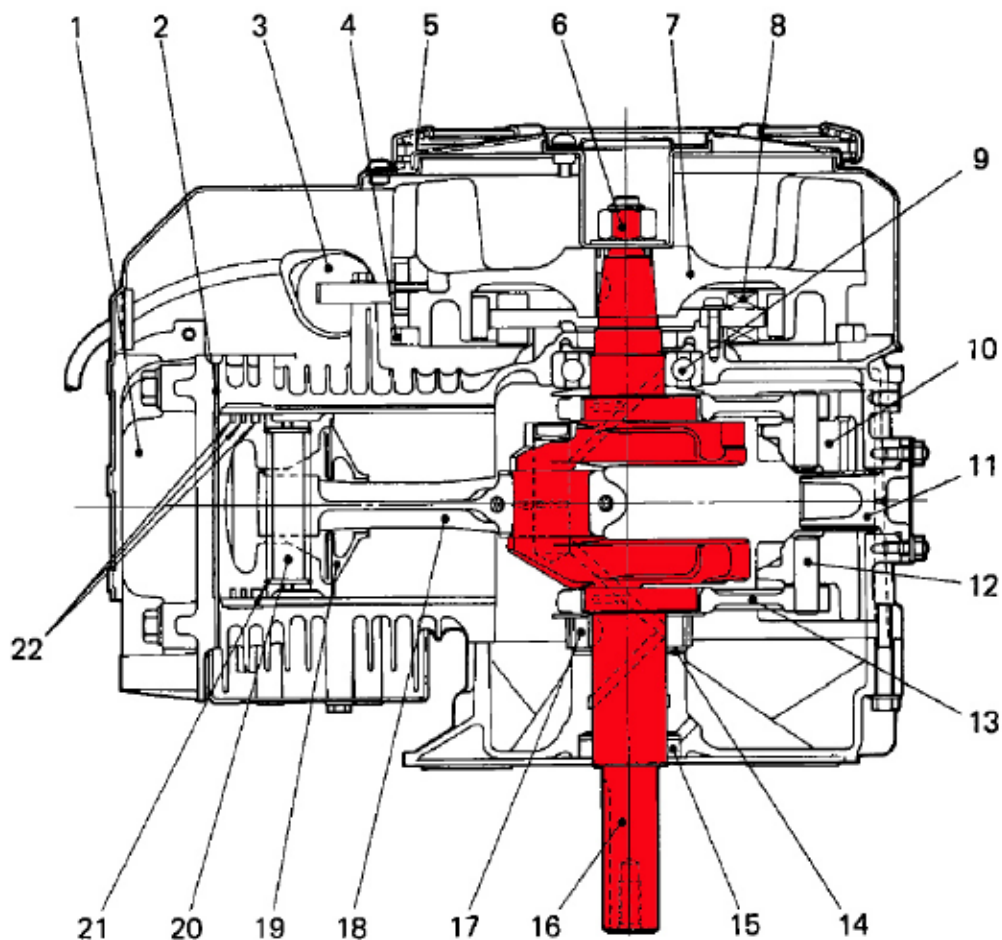


Figure 3.12 The forged steel crankshaft in engine assembly taken from the engine manual of forged crankshaft.

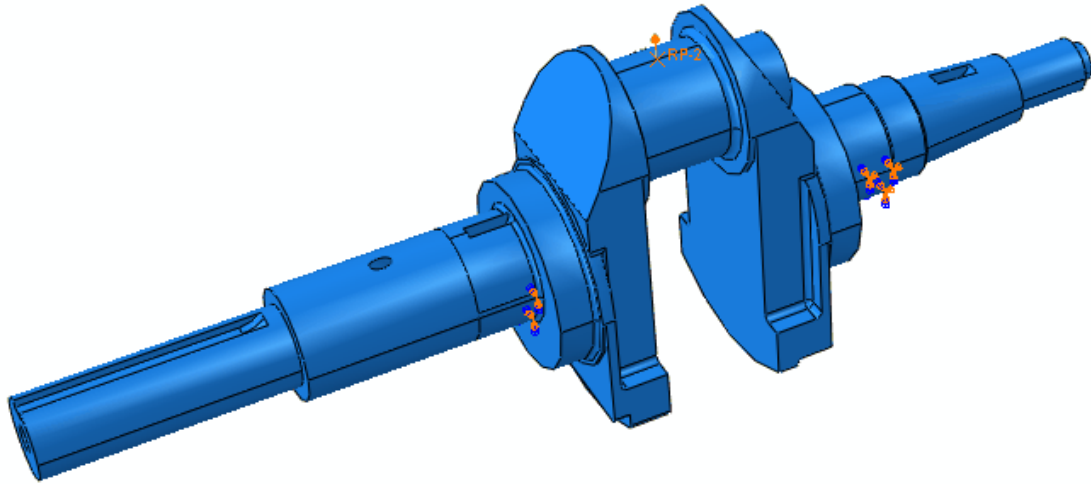


Figure 3.13 Load and Boundary conditions at '0' degree.

3.3 FEM Results

Finite element analysis was done for different angles with different forces. 11 numbers of angles were used for analysis as mentioned in section 3.2.

Section changes in the crankshaft geometry leads to stress concentrations at intersections. At the intersections, these edges are filleted but in spite of that these filleted areas are highly stressed. Therefore, stresses were traced over these locations.

Results and also investigations shows that highly stressed areas are fillets in the crankshaft during their service life. Therefore, six points on the fillets were selected and labelled in Figure 3.14 for forged steel crankshaft. Locations 1 and 6 are located on the boundary conditions. This loading condition is the only loading condition used at the time of maximum bending load, because at this time the torsional load is zero. Therefore, using the stress results and scaling them according to the maximum dynamic load at this moment will give the maximum stress at these locations.

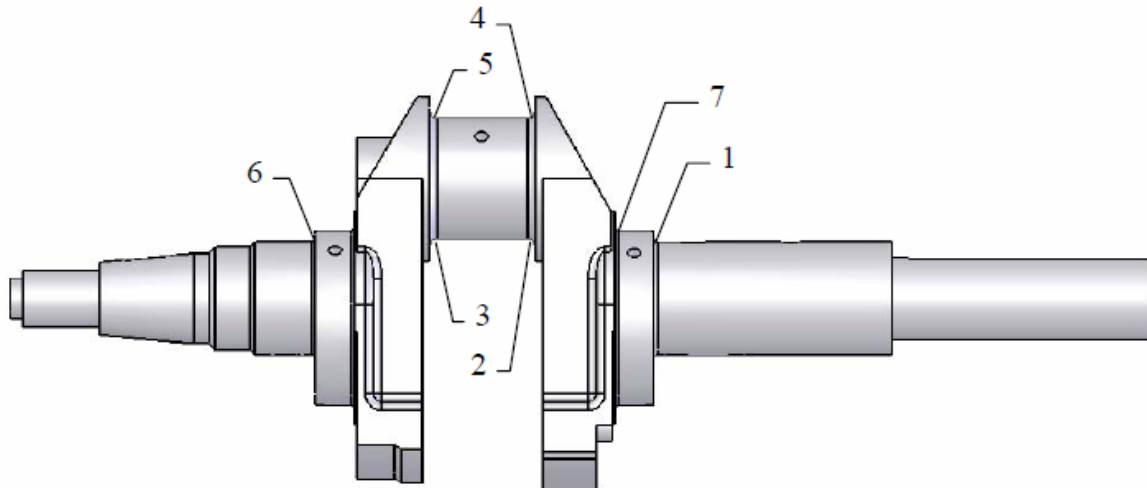
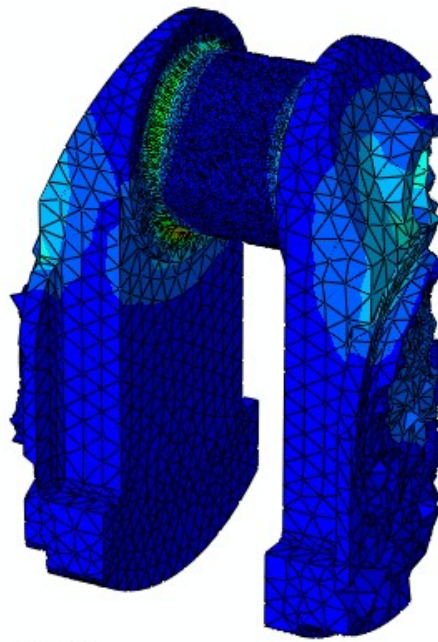


Figure 3.14 Critical locations on the forged crankshaft

It is found from many results that location 2 is the most critical one. According to the obtained results, the maximum von Mises stress value at location 2 for the forged steel crankshaft is 118 MPa at the engine speed of 3500 rpm. It is shown in figure 3.15.

One of the main objectives of performing the dynamic FE modeling was to determine the design loads for optimization of the forged steel crankshaft. The maximum load that is applied to the crankshaft during its service life is the load corresponding to the peak gas pressure. The maximum gas pressure occurs at about 355° crank angle. Also, the maximum stress occurs at this crank angle. Therefore, this loading condition is the most severe case of loading resulting in the maximum magnitude of von Mises stress at location 2.



W. Europe Daylight Time 2011

Figure 3.15 Maximum stress at the pin fillet and it is 118 MPa at the engine speed of 3500 rpm.

3.4 Liu-Zenner equivalent stresses

As mentioned in the CAO procedure, we need to find equivalent Liu-Zenner stresses on the corresponding nodes from the critical shape. From FE results and many research papers it is known that fillet areas at the pin surface are prone to fatigue crack formation. So in this study we considered two sets of fillets on the pin (shown in figure 3.16) for the calculation of equivalent Liu-Zenner stresses on the corresponding nodes. We can use python or Matlab for finding out Liu-Zenner stresses. In this study we have used Matlab code.

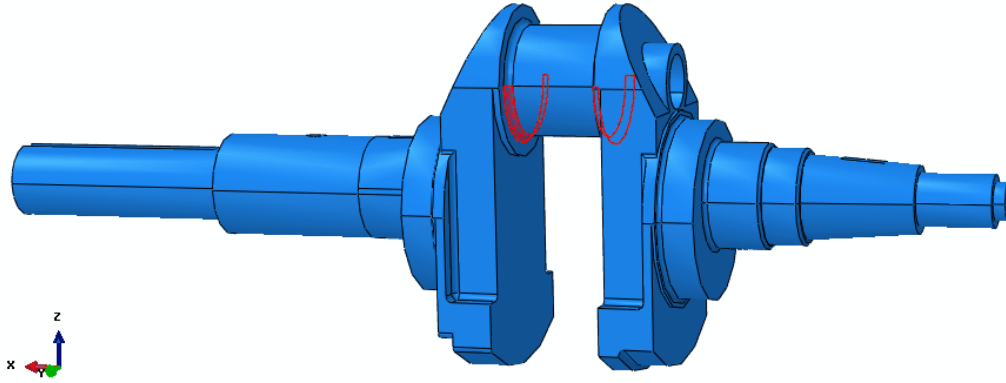


Figure 3.16 Critical fillet locations for shape modification

3.5 Virtual temperature distribution

These found equivalent Liu-Zenner stresses are applied as virtual temperature on the nodes in each fillet sets. During this analysis load is considered as zero. Mean value of the Liu-Zenner stresses is considered as an initial value for thermal analysis. Proper material properties are assigned required for thermal analysis. Conductivity, specific heat and thermal expansion coefficient are mainly of them. Thermal expansion coefficient is set such that $\alpha > 0$, to only heated region. The Growth Zone which previously experienced the highest loads, at this stage is subjected to the highest temperature variations and consequently expands more.

The results are shown in the figure 3.17 and figure 3.18.

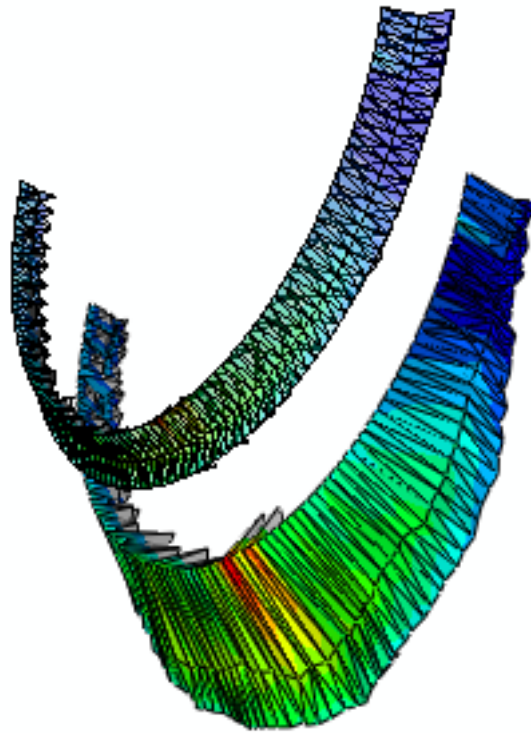


Figure 3.17 Shows the thermal distribution on nodes and change in shape. Original and deformed, both shapes are shown.

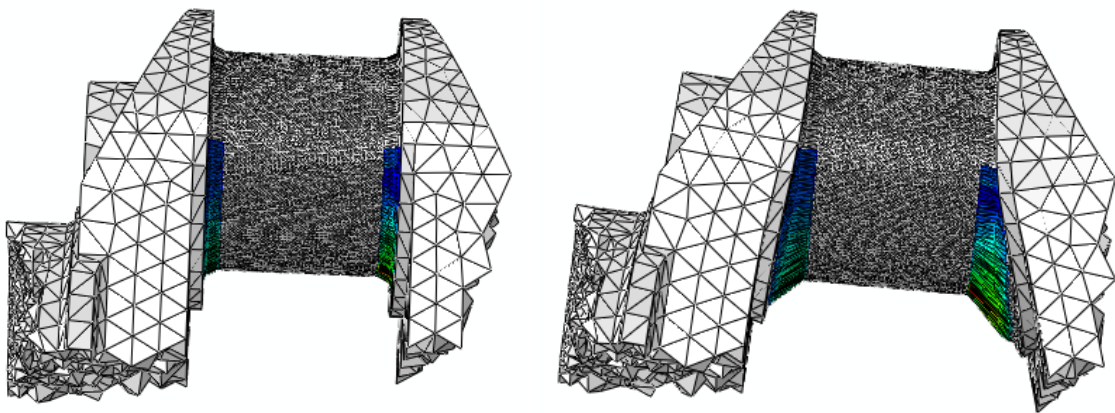


Figure 3.18 Shows both sets in un-deformed and deformed shapes.

3.6 Applying nodal displacements

After thermal analysis displaced co-ordinates of the nodes on critical curve are extracted. These displaced node co-ordinates are used build new 3d model. On the new 3d model the same sequence of dynamic loading is followed. Results show low stress at the critical location. So the displaced nodal co-ordinates modify the critical shape to lower the stress concentration.

3.7 Convergence

In our analysis at the 4th iteration we found that both von-mises and Liu-Zenner stresses are increasing. So the result at the 3rd iteration is the final results. Due to shape modification at critical location, the von-mises stress is reduced to 116.079 from 118.2. Both figures of Von-mises and Liu-Zenner stress convergence are shown in the figure 3.19 and 3.20 respectively.

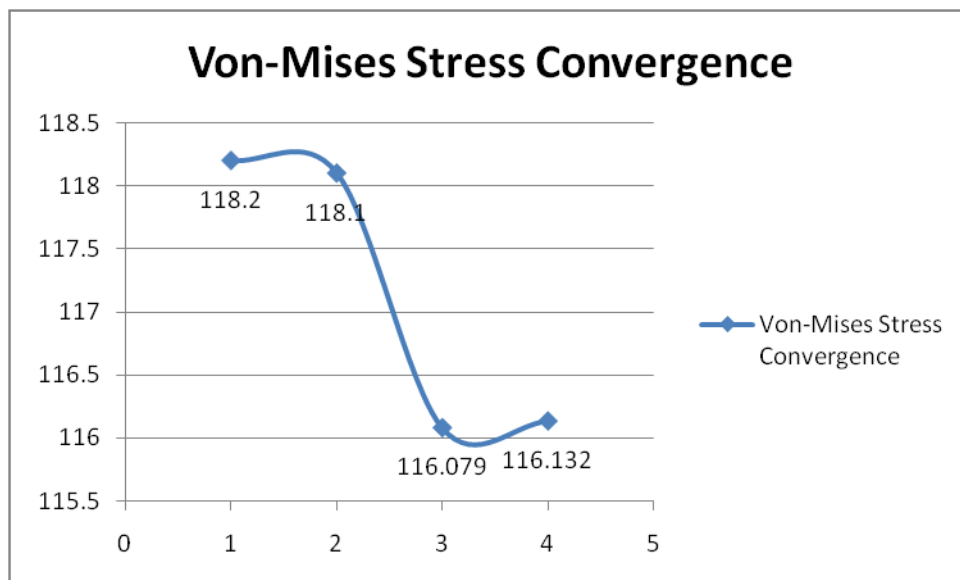


Figure 3.19. Von-Mises stress convergence

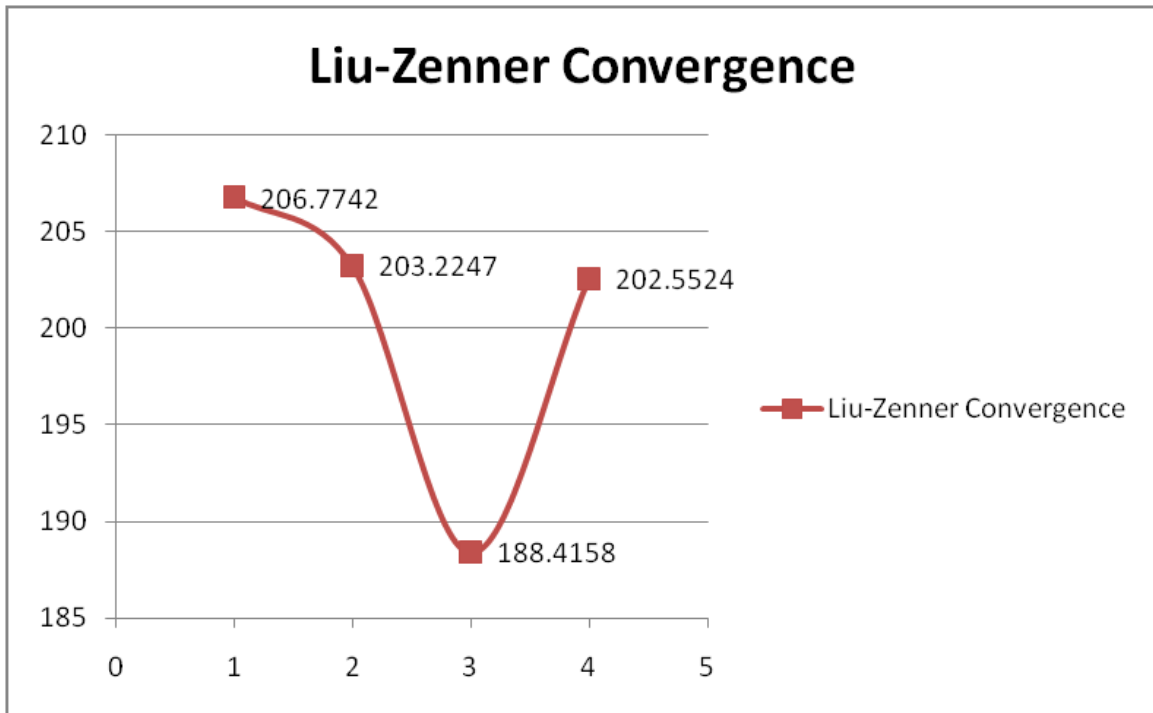


Figure 3.20 Liu-Zenner stress convergence

4. Conclusion

This developed method of optimization is very useful over other available methods for optimization of shape under the Multi-axial loading. We can make following concluding points;

1. A novel optimization method has been presented for modifying a notched geometry under multi-axial fatigue loading. The optimization process is based on the CAO (Computer Aided Optimization) proposed by Mattheck, modified by adopting the Liu–Zenner fatigue criterion instead of a static criterion.

2. The Mean Point Method was developed to determine the minimum circumscribe circle: this algorithm shows a better computational efficiency with respect to the existing methods.

3. A numerical routine is developed that, by means of interfaces to the ABAQUS FE code, is able to lead to an optimized geometry of notch details under general multi-axial loading.

4. The results of the presented example, optimized by this process, show a notable improvement in the fatigue equivalent Liu–Zenner stress distribution along the notch contour. According to the obtained results the method is found to be applicable to a wide range of loading and geometry combinations. Furthermore it is very fast with respect to the number of iterations.

5. Due to the complexity of the subject, it is to be mentioned that an experimental verification is necessary to validate the process and its results.

References

- [1] R. Ghelichi, A. Bernasconi, M. Guagliano. Geometrical optimization of notches under multi-axial fatigue loading.
- [2] Jiping Liu and Harald Zenner. Fatigue limit of ductile metals under multi-axial loading.
- [3] Jan Papuga. A survey on evaluating the fatigue limit under multi-axial loading.
- [4] José C. Balthazar and Lucival Malcher. A review on the main approaches for determination of the multi-axial high cycle fatigue strength.
- [5] F. Ellyin, K.Golos, Z.Xia. In-Phase and Out-of-Phase Multi-axial Fatigue.